NANO LETTERS

Letter

pubs.acs.org/NanoLett

# Compensation of Coulomb Blocking and Energy Transfer in the Current Voltage Characteristic of Molecular Conduction Junctions

Guangqi Li,*[,†] Manmohan S. Shishodia,[‡,§] Boris D. Fainberg,[‡,§] Boris Apter,[∥] Michal Oren,[§] Abraham Nitzan,[§] and Mark A. Ratner[†,#]

[†]Non-Equilibrium Energy Research Center (NERC), Northwestern University, Evanston, Illinois 60208, United States

[‡]Faculty of Science, Holon Institute of Technology, 58102 Holon, Israel

[§]School of Chemistry, Tel-Aviv University, 69978 Tel-Aviv, Israel

[∥]Engineering Faculty, Holon Institute of Technology, 58102 Holon, Israel

[#]Department of Chemistry, Northwestern University, Evanston, Illinois 60208, United States

Supporting Information

**ABSTRACT:** We have studied the influence of both exciton effects and Coulomb repulsion on current in molecular nanojunctions. We show that dipolar energy-transfer interactions between the sites in the wire can at high voltage compensate Coulomb blocking for particular relationships between their values. Tuning this relationship may be achieved by using the effect of plasmonic nanostructure on dipolar energy-transfer interactions.

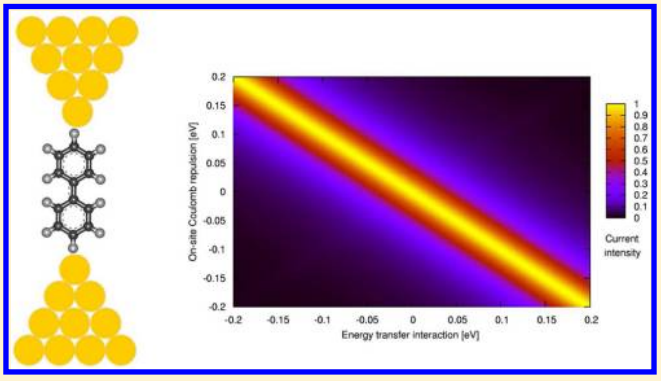


**KEYWORDS:** *Molecular conduction nanojunctions, exciton effects, energy transfer, Coulomb blocking, plasmonic effects*

Electron transport through molecular wires has been under intense theoretical[1−5] and experimental[6−8] study. Energy-transfer interactions can sometimes have important effects on the dynamics of such processes. Charge and energy transfer in a linear 2,2′:6′,2″-terpyridine-based trinuclear Ru-(II)-Os(II) nanoscale array[9] and one-dimensional energy/electron transfer along amylose-encapsulated chain chromophores[10] are examples. In addition, it seems likely that energy transfer takes place in chemically responsive molecular transistors based on a dimer of terpyridyl molecules chelating with $Co^{2+}$.[11] We have recently developed a theory of electron transport through molecular wires in the presence of intersite dipolar energy-transfer interactions in the wire, using a model comprising a bridge with two two-level sites connecting free electron reservoirs.[12,13] Our calculations show that for noninteracting electrons, this structure leads to reduction in the current at high voltage for a homodimer bridge. This effect, called "exciton blocking", disappears for strong on-site Coulomb repulsions.[13]

Although in free exciton systems, dipolar interactions ($\lesssim$ 0.01−0.1 eV)[14] are considerably smaller than on-site Coulomb interaction $U$ (characteristically $U \sim 1$ eV);[15] the former may still have strong effects under some circumstances, e.g., in the vicinity of metallic structures in or near the nanojunctions. In such cases dipolar interactions may be enhanced, while Coulomb interaction is screened.[16−19] The question "how do such dipolar interactions affect the junction transport properties when they are of the same order of magnitude as on-site Coulomb repulsion $U$?" can become pertinent.

In this letter we consider the simultaneous effects of energy (exciton) transfer and Coulomb repulsion on the conduction properties of molecular nanojunctions. We evaluate the enhancement of dipolar energy-transfer near plasmonic nanostructures and show that the magnitude of the enhanced interaction can approach $U$. We then show that this interaction, $J$, can have a substantial effect on the transport and can in fact substantively reduce the high-voltage Coulomb blocking effect for particular values of $J$ and $U$.

We consider a spinless molecular wire model that comprises two interacting sites (each represented by its ground, $|g\rangle$, and excited, $|e\rangle$, states) positioned between two leads. The latter are represented by free electron reservoirs L and R (Figure 1), characterized by the electronic chemical potentials $\mu_K$, $K$ = L, R, and by the ambient temperature $T$. The corresponding Fermi distributions are $f_K(\varepsilon_k) = [\exp((\varepsilon_k - \mu_K)/k_BT) + 1]^{-1}$, and the

**Received:** November 23, 2011
**Revised:** March 14, 2012
**Published:** March 30, 2012

  

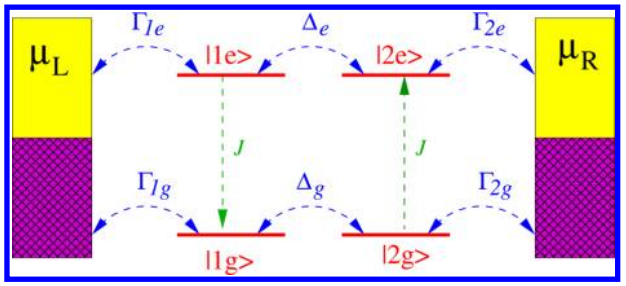


**Figure 1.** A model for energy-transfer induced effects in molecular conduction. The molecular bridge is a dimer, where each site is represented by its ground, $|1g\rangle$ and $|2g\rangle$, and excited, $|1e\rangle$ and $|2e\rangle$, levels with the nearest-neighbor site coupling $\Delta_g$ and $\Delta_e$. The two metal leads characterized by electrochemical potentials $\mu_R$ and $\mu_L$ are coupled to their nearest molecular site with the transfer rate $\Gamma_{2e}$, $\Gamma_{2g}$, $\Gamma_{1e}$, $\Gamma_{1g}$. $J$ represents exciton hopping.

difference $\mu_L - \mu_R = eV_{bs}$ is the imposed voltage bias. The corresponding Hamiltonian is

$$H = H_{wire} + H_{leads} + H_{int} \equiv H_0 + H_{int} \tag{1}$$

$$H_{leads} = \sum_{k\in\{L,R\}} E_k c_k^\dagger c_k \tag{2}$$

$$H_{wire} = \sum_{\substack{m=1,2\\ f=g,e}} E_{mf} c_{mf}^\dagger c_{mf} - \sum_{f=g,e} \Delta_f (c_{2f}^\dagger c_{1f} + c_{1f}^\dagger c_{2f}) + \hbar(J b_1^\dagger b_2 + \text{H.c.}) + \frac{U}{2} \sum_{m=1,2} N_m(N_m - 1) \tag{3}$$

$$H_{int} = \sum_{mf,k\in K_m} V_k^{(mf)} c_k^\dagger c_{mf} + \text{H.c.} \tag{4}$$

where $c_{mf}^\dagger$ ($c_{mf}$) ($m$ = 1, 2; $f$ = g, e, see Figure 1) are creation (annihilation) operators for electrons in the different site states of energies $E_{mf}$, while $c_k^\dagger$ ($c_k$) ($k \in$ L, R) are creation (annihilation) operators for free electrons (energies $E_k$) in the leads L and R. The occupation operators are $n_{mf} = c_{mf}^\dagger c_{mf}$ for the different site states, and site occupation operators are given by $N_m = n_{mg} + n_{me}$. The operators $b_m^\dagger = c_{me}^\dagger c_{mg}$ and $b_m = c_{mg}^\dagger c_{me}$ are exciton creation and annihilation operators on the molecular sites $m$ = 1, 2. In eq 3, $\Delta_f$ represents electron tunneling between site states of similar energies (i.e., between $|g\rangle$ levels of sites 1 and 2 and between $|e\rangle$ levels on these sites), the $J$ terms represent exciton hopping (energy transfer) between molecular sites, and the $U$ terms correspond to on-site Coulomb interactions. The molecule–leads interaction $H_{int}$ describes electron transfer between the molecular bridge and the leads that gives rise to net current in the biased junction. In eq 4, $K_m$ is the lead closer the molecular site $m$ ($K_1$ = L, $K_2$ = R), and H.c. denotes a Hermitian conjugate. Below we will also use the population operators $\lambda_f = n_{1f} + n_{2f}$ in the manifolds of ground ($f$ = g) and excited ($f$ = e) site levels.

Our analysis is based on the generalized master equation for the reduced density matrix of the molecular subsystem,[12,13] obtained using a standard procedure[20−22] based on taking $H_{int}$ as a perturbation. Briefly, one starts with the equation for the total density operator and uses the projectors $P_K$ of the type $P_K\rho(t) = \rho_K \text{Tr}_K \rho(t)$ with $\rho_K$ being the density matrix of the leads in their equilibrium state, in order to derive an equation for the time evolution of the reduced density matrix $\sigma = \text{Tr}_R\text{Tr}_L\rho$. This leads to[13]

$$\frac{d\sigma(t)}{dt} = -\frac{i}{\hbar}[H_{wire}, \sigma(t)] - \frac{1}{\hbar^2}\text{Tr}_K \int_0^\infty d\tau [H_{int}, [H_{int}^{int}(-\tau), \rho(t)]] \tag{5}$$

where $\text{Tr}_K = \text{Tr}_R\text{Tr}_L$ and $H_{int}^{int}(-\tau) = \exp(-iH_0\tau/\hbar)H_{int}\exp(iH_0\tau/\hbar)$ is the interaction representation of $H_{int}$. The second term on the right-hand side of eq 5 can be evaluated in the Markovian and wide-band limits and is in terms of the rate constant of charge transfer from state $f$ of site $m$ to the corresponding lead:

$$\Gamma_{mf} = \frac{2\pi}{\hbar} \sum_{k\in K_n} |V_k^{(mf)}|^2 \delta(E_k - E_{mf}) \tag{6}$$

The resulting rate equation can be solved numerically.

The electric current $I$ is defined as the current going into the system on the left side, using the electron number operator of the left lead $N_L = \sum_{k\in L} c_k^\dagger c_k$,[22,23]

$$I(t) = \text{Tr}\left\{|e|\frac{d}{dt}\sum_{k\in L} c_k^\dagger c_k \rho(t)\right\} \tag{7}$$

that at steady state is equal to the current going out of the system on the right.

In this calculation we use the following parameters: $E_{1g} = E_{2g} \equiv E_g = 0$, $E_{1e} = E_{2e} \equiv E_e = 2$ eV, $\Delta_g = \Delta_e = 0.01$ eV, $\Gamma_{1f} = \Gamma_{2f} = \Gamma = 0.02$ eV for $f$ = g, e (below we use $\Gamma$ to denote the order of magnitude of these widths) and $T$ = 100 K. The leads chemical potentials in the biased junction were taken to align symmetrically with respect to the energy levels $E_{1g}$ and $E_{1e}$, i.e., $\mu_L = (E_{1g} + E_{1e} + V_{bs})/2$ and $\mu_R = \mu_L - V_{bs}$. We also used the value of $I_0$ = e × 0.01 eV/$\hbar$ = 2.45 × $10^{-6}$ A as the unit of current $I$.

Figures 2 and 3 show the current as a function of the parameters of Coulomb interaction $U$ and the dipole–dipole

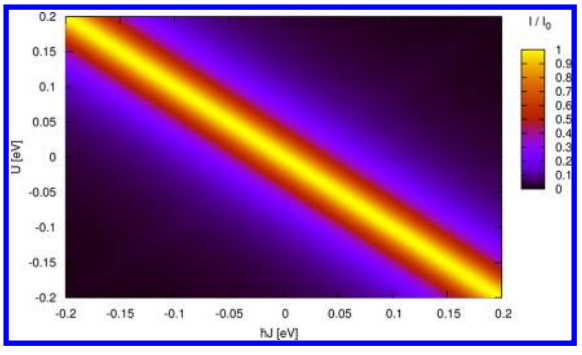


**Figure 2.** Current $I$ displayed as function of the energy-transfer coupling $J$ and on-site interaction $U$. The current shows a maximum at $U = -\hbar J$ with the same peak value $I/I_0$ = 1. The bias voltage $V_{bs}$ = 4.0 eV, and $\Delta_g = \Delta_e$ = 0.01 eV.

interaction $J$ between sites and as a function of the imposed voltage bias for different values of $J$ and $U$, respectively. For $J$ = 0, Figures 2 and 3 show the effect of Coulomb blocking: current has a maximum at $U$ = 0 and decreases with increasing $U$. For $U$ = 0, the figures show the effect of "exciton blocking" (as predicted in ref 13): current has a maximum at $J$ = 0 and decreases with increasing the absolute value of $J$. The most remarkable observation is however the mutual compensation of exciton and Coulomb blocking seen in Figures 2 and 3, where the current in Figure 2 goes through a maximum at $U = -\hbar J$ with a $U$-independent peak value $I/I_0$ = 1. Remarkably, if either $\Delta_g$ or $\Delta_e$ are taken to zero (Figure 4), we observe peaks for both $U = -\hbar J$ and $U = \hbar J$.


dx.doi.org/10.1021/nl204130d | Nano Lett. 2012, 12, 2228–2232

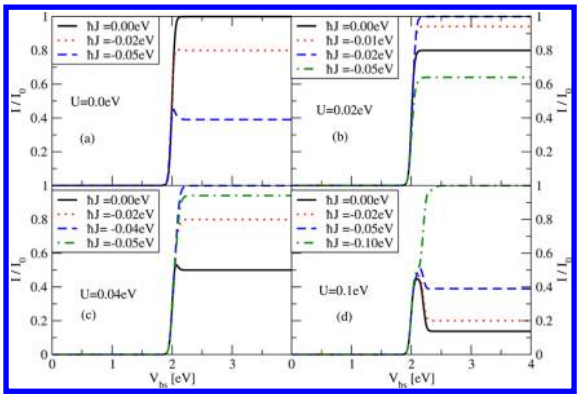


**Figure 3.** Current $I$ displayed as a function of bias voltage $V_{bs}$ for different $J$ and $U$. Since we assume a symmetric bias voltage, the energy level will be in the open window when the bias voltage achieves 2 eV, since we took 2 eV as $E_e - E_g$, where we see a jump shoulder of the current. The current shows its maximum value at $U = -\hbar J$, and $\Delta_g = \Delta_e = 0.01$ eV.

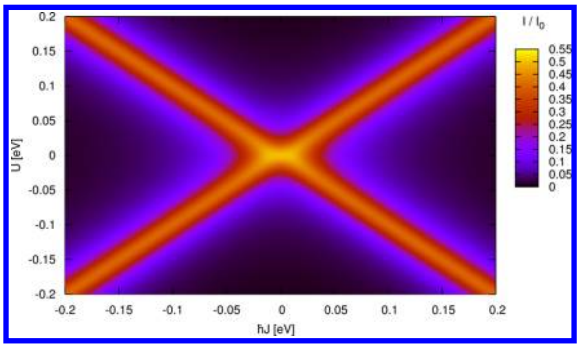


**Figure 4.** Current $I$ displayed as function of the energy-transfer coupling $J$ and on-site interaction $U$ for $\Delta_g = 0$ and $\Delta_e = 0.01$ eV. The current goes through a maximum at $U = \pm\hbar J$. The bias voltage $V_{bs} = 4.0$ eV. The same results are obtained when $\Delta_g = 0.01$ eV and $\Delta_e = 0$.

To understand this behavior, we extend the analytical evaluation of ref 13 to include finite on-site Coulomb repulsion between charge carriers. Details can be found in ref 13 and in the Supporting Information. Since the total molecular populations described by operators $\lambda_f$ are conserved under the unitary transformations associated with the diagonalization of $H_{wire}$,[13] the total $2^4 \times 2^4$ occupation state-space can be partitioned into nine smaller subspaces (see Figure 2 of ref 13): four one-dimensional subspaces for $[\lambda_f] = 0, 2$ for either $f = e, g$ (type I); four two-dimensional subspaces for $[\lambda_f] = 1$ and $[\lambda_{f'}] = 0, 2$, where $f \neq f'$ (type II); and one four-dimensional subspace for $[\lambda_e] = [\lambda_g] = 1$ (type III). Here we use $[\lambda_f]$ to denote the eigenvalues of matrix operator $\lambda_f$. The type I submatrix is diagonal, while four pairs of states with each pair coupled by the charge-transfer interaction are associated with the four $2 \times 2$ blocks of the type II subspace. The four type III states are coupled by both the charge- and exciton-transfer interaction and constitute the $4 \times 4$ block of subspace III.

This partitioning can be exploited to diagonalize the kinetic matrix and evaluate the current through the junction. For $J < 0$ ($J$ aggregates) the current can be shown to be given by

$$I = -\frac{2e}{\hbar}\Delta_e \mathrm{Im}\{[\sigma_{32}(\mathrm{III}) + \sigma_{41}(\mathrm{III})]\cos\phi + [\sigma_{31}(\mathrm{III}) - \sigma_{42}(\mathrm{III})]\sin\phi - \sum_{[\lambda_g]=0,2} \sigma_{-+}(\mathrm{II};\, [\lambda_e]=1,\, [\lambda_g])\} \quad (8)$$

with

$$\phi = \frac{1}{2}\mathrm{arccot}\frac{U^2 - J^2\hbar^2 + 4\Delta_e^2}{4\Delta_e J\hbar} \quad (9)$$

and the reduced density matrix $\sigma$ shown in eq 5. Equations 8 and 9 are the generalizations of eqs 32 and 33 of ref 13 to finite on-site Coulomb repulsion. The matrix−element indices "+" and "−" in eq 8 label the eigenstates of the wire Hamiltonian in subspaces II, and indices 1−4 are the corresponding labels in subspace III. The nondiagonal elements of the density matrix on the right-hand side of eq 8 can be evaluated using eq D2 of ref 13: $\mathrm{Im}\sigma_{\alpha\beta} \sim -(E_\alpha - E_\beta)\hbar\Gamma/(E_\alpha - E_\beta)^2 + 4\hbar^2\Gamma^2$, where $E_\alpha$ and $E_\beta$ are eigenstate energies of $H_{wire}$, and $\Gamma$ is of the order of the relaxation parameter, eq 6. In particular, we get the same contribution from the third summation term on the right-hand side of eq 8, as in case of $U = 0$ (eq 41 of ref 13):

$$\frac{2e}{\hbar}\Delta_e \mathrm{Im}\sum_{\lambda_g=0,2}\sigma_{-+} \sim \frac{2e\Gamma}{1 + \hbar^2\Gamma^2/\Delta_e^2} \quad (10)$$

Let us evaluate the contributions of the first and the second terms on the right-hand side of eq 8 at $U^2 = J^2\hbar^2$, corresponding to maxima shown in Figure 4. The corresponding energy differences between the states of subspace III are given by

$$\begin{aligned} E_1 - E_4 &= \Delta_e - J\hbar - \sqrt{\Delta_e^2 + J^2\hbar^2} \\ E_2 - E_3 &= -\Delta_e - J\hbar + \sqrt{\Delta_e^2 + J^2\hbar^2} \\ E_1 - E_3 &= \Delta_e - J\hbar + \sqrt{\Delta_e^2 + J^2\hbar^2} \\ E_4 - E_2 &= \Delta_e + J\hbar + \sqrt{\Delta_e^2 + J^2\hbar^2} \end{aligned} \quad (11)$$

and

$$\sin\phi,\ \cos\phi = \frac{1}{\sqrt{2}}\sqrt{1 \pm \frac{\Delta_e}{\sqrt{\Delta_e^2 + J^2\hbar^2}}} \quad (12)$$

When $\hbar|J| \ll \Delta_e$, eq 12 yields $\cos\varphi \approx 0$, $\sin\varphi \approx 1$, and only the second term in eq 8 gives a contribution to the current from the states of subspace (III). Under this condition one gets using eq 11

$$\frac{2e}{\hbar}\Delta_e \mathrm{Im}[\sigma_{31} - \sigma_{42}] \sim \frac{e\Gamma}{1 + \hbar^2\Gamma^2/\Delta_e^2} \quad (13)$$

This contribution is of the same order of magnitude as that from the states of subspaces (II), eq 10.

In the opposite case, $\hbar|J| \gg \Delta_e$, $\cos\varphi \approx \sin\varphi \approx 1/\sqrt{2}$, and both first and second terms in eq 8 contribute to the current. For this case using eq 11 we get

$$\frac{2e}{\hbar\sqrt{2}}\Delta_e \mathrm{Im}[\sigma_{32} + \sigma_{41} + \sigma_{31} - \sigma_{42}] \sim \frac{2\sqrt{2}\,e\Gamma}{1 + 4\hbar^2\Gamma^2/\Delta_e^2}$$

This contribution is of same order of magnitude as those of eqs 10 and 13. In other words, in the case under consideration, a simultaneous change in the values of $J$ and $U$ for $U^2 = J^2\hbar^2$ does not affect the current. This stands in contrast to the separate effects of exciton coupling and Coulomb repulsion.[13] In a sense this is an "exciton compensation" of the Coulomb blocking (ECCB) effect on electron transmission through the bridge.

Anticipating the discussion below on the possibility for controlling the value of $J$ by manipulating the electromagnetic


dx.doi.org/10.1021/nl204130d | Nano Lett. 2012, 12, 2228−2232

environment of the junction using plasmonic response of the metal contact, we address the possibility of complex-valued $J$ due to coupling to the plasmonic resonances involving decay processes. The latter, as is known, is described by the imaginary part of interaction. Figure 5 shows that the ECCB phenomenon

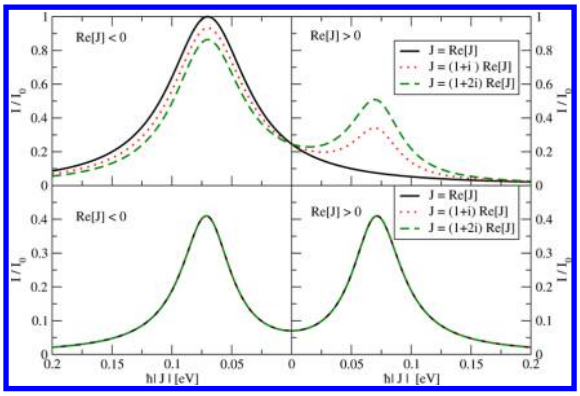


**Figure 5.** Current $I$ displayed as a function of $|J|$ for complex-valued $J$ when $U$ = 0.07 eV. All the lines have their peaks at the position $\hbar|J| = U$, while $\Delta_g$ = 0.01 eV and $\Delta_e$ = 0.01 eV (upper two panels), and $\Delta_g$ = 0.01 eV and $\Delta_e$ = 0.0 (bottom two panels). The bias voltage is $V_{bs}$ = 4.0 eV.

is conserved for complex-valued $J$ with maximum current obtained at $U = \pm \hbar|J|$, depicting additional maxima with respect to the case of real $J$. These figures also demonstrate that the relevant magnitude for complex-valued $J$ is its modulus, $|J|$.

It is interesting to examine possible experimental setups in which ECCB may be realized. In free space, $U$ is considerably larger than $J$. On the other hand, dipolar energy transfer is known to be effected by proximity to plasmonic metal structures. Coulomb repulsion is affected by metal screening, but for our geometry, the effect is relatively small. We assume that the site (point dipole) is found at the distance of 1 nm from the nearest metal lead (if the distance is less, the classical description of the plasmonic effects is incorrect). If an extra electron is placed on the site, the distance between the site's electrons is about 0.1 nm (the atom size). The (positive) image of the extra electron of the site is in the metal lead at the distance of 1 nm from the metal surface. This means that the distance between the extra electron of the site and its image is 2 nm, much larger than the inter-electron distances between the site's electrons. Therefore, the metal screening of the Coulomb repulsion is small, for the distances considered here. In contrast to $U$, the energy-transfer coupling $J$ can be controlled by the electromagnetic environment. This can in principle be achieved via the plasmonic response of the metallic contacts, that can greatly alter the effective dipole−dipole interactions in the molecular bridge.[16−19] To demonstrate this, we have calculated the energy-transfer coupling in the gap between two metal nanospheres by the finite-difference time-domain (FDTD) method. We used commercially available FDTD Solutions software by Lumerical.[28] This is shown in Figure 6. For comparison, we also show the results calculated within the quasistatic approximation[17,18,24,25] for a single nanosphere (the right sphere in the inset to Figure 6 is absent) (the calculational details can be found in ref 27). The metal particles are represented by a Drude dielectric model, $\varepsilon = \varepsilon_0 - \omega_p^2/[\omega(\omega + i\gamma)]$ with parameters $\varepsilon_0$ = 3.57, $\omega_p$ = 9.1 eV, and $\gamma$ = 0.052 eV corresponding to silver; the host medium was taken as

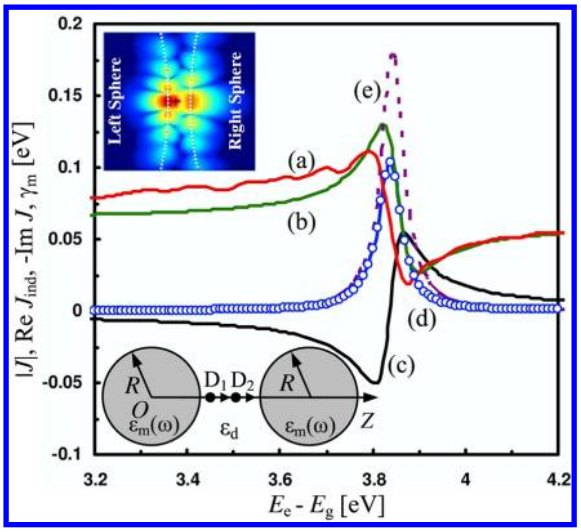


**Figure 6.** The dipole−dipole interaction $|J|$ in the gap of the dimer of silver spheres of radius of $R$ = 50 nm as a function of energy difference between the excited and ground molecular states (curve a). The metallic nanosystem is described through a frequency-dependent dielectric function $\varepsilon_m(\omega)$ and assumed to be embedded in a host medium characterized by its dielectric permittivity $\varepsilon_d$. Two point dipoles $D_1$ and $D_2$ with dipole moments of 10 D are situated in the dimer axis and directed along it in the same direction (see lower inset). The dipoles are placed at a distance of 1 nm from each other, and the distance between a sphere surface and the nearest dipole is 1 nm. The upper inset shows a 2 D distribution of electric field intensity, induced by the left dipole at 3.8 eV. The field enhancement due to plasmon excitation inside the gap can be clearly seen. We also show the calculation results for a single nanosphere (the right sphere in the lower inset is absent): $|J|$ (curve b), Re$J_{ind}$ (curve c), −Im$J$ (curve d), and the energy-transfer rate from the nearest dipole to metal $\gamma_m$ (curve e). Here $J_{ind}$ denotes the part of $J$ induced by a nanosphere. Curve Re$J$ should be shifted below with respect Re$J_{ind}$ on the value of the dipole−dipole interaction in free space (−0.06125 eV). The Fano-like peaks at 3.8 eV mirror the plasmonic resonance.

transparent with $\varepsilon_d$ = 2. Figure 6 shows enhancement of dipole−dipole interactions ($J$) both in the gap of a dimer of silver spheres and near the single sphere as a function of the transition frequency $|e\rangle \rightarrow |g\rangle$.

It appears that proximity to plasmonic structures can indeed be used to enhance energy transfer to the level needed to observe ECCB, however to complete this assessment, we also need to consider metal-induced damping of excitation energy. To this end, we evaluated the rate of the energy transfer to metal $\gamma_m$ for a single sphere, using the approaches from refs 17 and 18, which is shown in Figure 6 together with $|J|$. One can see that due to different frequency dependence of $|J|$ and $\gamma_m$, rather large values of $|J|$ can be induced at frequencies for which $\gamma_m \ll |J|$.

In conclusion, the coexistence of electron and energy-transfer interactions in molecular junctions may result in a new effect: ECCB of electron transmission at high voltage. ECCB can permit efficient electron transport even in systems with strong Coulomb repulsion for carriers and can be realized by controlling the plasmonic response of metallic contacts. Here the enhancement of the dipole−dipole interaction calculated using FDTD simulation for the dimer of silver spheres, and within the quasistatic approximation for a single sphere, reached the value of 0.13 eV for nanosphere-shaped metallic contacts. It is conceivable that more realistic geometries of the


dx.doi.org/10.1021/nl204130d | Nano Lett. 2012, 12, 2228−2232

contacts, like the bowtie antenna,[26] etc., will give a larger enhancement. This issue will be studied elsewhere.

## ■ ASSOCIATED CONTENT

### Supporting Information

This material is available free of charge via the Internet at http://pubs.acs.org.

## ■ AUTHOR INFORMATION


### Corresponding Author

*E-mail: guangqili@northwestern.edu


### Notes

The authors declare no competing financial interest.

## ■ ACKNOWLEDGMENTS

Authors are supported by the Non-Equilibrium Energy Research Center (NERC) which is an Energy Frontier Research Center funded by the U.S. Department of Energy, Office of Science, Office of Basic Energy Sciences under award number DE-SC0000989 (G.L. and M.R.), the Israel Science Foundation grant no. 1646/08, the Germany−Israel Foundation, the European Research Council under the European Union's Seventh Framework Program (FP7/2007-2013; ERC grant agreement no. 226628) (A.N.), the Israel−U.S. Binational Science Foundation (A.N. and B.F.), and the Russia−Israel Scientific Research Cooperation (B.F.).

## ■ REFERENCES


(1) Nitzan, A.; Ratner, M. A. *Science* **2003**, *300*, 1384.
(2) Ventra, M. D. *Electrical Transport in Nanoscale Systems*; Cambridge University Press: Cambridge, 2008.
(3) Galperin, M.; Ratner, M. A.; Nitzan, A.; Troisi, A. *Science* **2008**, *319*, 1056.
(4) Cuevas, J. C.; Scheer, E. *Molecular electronics: an introduction to theory and experiment*; World Scientific Publishing Company, Inc.: Trenton, NJ, 2010.
(5) Datta, S. *Quantum Transport: Atom to Transistor*; Cambridge University Press: Cambridge, U.K., 2005.
(6) Chen, F.; Tao, N. J. *Acc. Chem. Res.* **2009**, *42*, 429.
(7) Heath, J. R. *Annu. Rev. Mater. Res.* **2009**, *39*, 1.
(8) Cuniberti, G.; Fagas, G.; , Richter, K. *Introducing Molecular Electronics*; Springer: Heidelberg, Germany, 2005.
(9) Benniston, A. C.; Harriman, A.; Li, P.; Sams, C. A. *J. Am. Chem. Soc.* **2005**, *127*, 2553.
(10) Kim, O.-K.; Je, J.; Melinger, J. S. *J. Am. Chem. Soc.* **2006**, *128*, 4532.
(11) Tang, J.; Wang, Y.; Nuckolls, C.; Wind, S. J. *J. Vac. Sci. Technol. B* **2006**, *24*, 3227.
(12) Fainberg, B. D.; P. Hänggi, Kohler, S.; Nitzan, A. Proceedings of the International Conference on Transport and Optical Properties of Nanomaterials (ICTOPON), Allahabad, India, January 5−8, 2009; Singh, M. R., Lipson, R. H., Eds.; American Institute of Physics: Melville, NY, 2009; *1147*, 78.
(13) Li, G.-Q.; Fainberg, B. D.; Nitzan, A.; Kohler, S.; Hänggi, P. *Phys. Rev. B* **2010**, *81*, 165310.
(14) Mukamel, S.; Abramavicius, D. *Chem. Rev.* **2004**, *104*, 2073.
(15) Thomann, H.; Dalton, L. R.; Grabowski, M.; Clarke, T. C. *Phys. Rev. B* **1985**, *31*, 3141.
(16) Gersten, J. I.; Nitzan, A. *Chem. Phys. Lett.* **1984**, *104*, 31.
(17) Hua, X. M.; Gersten, J. I.; Nitzan, A. *J. Chem. Phys.* **1985**, *83*, 3650.
(18) Durach, M.; Rusina, A.; Klimov, V. I.; Stockman, M. I. *New J. of Phys.* **2008**, *10*, 105011.
(19) Schatz, G. C.; VanDuyne, R. P. *Surf. Sci.* **1980**, *101*, 425.
(20) Kohler, S.; Lehmann, J.; Hänggi, P. *Phys. Rep.* **2005**, *406*, 379.
(21) Kaiser, F. J.; Strass, M.; Kohler, S.; Hänggi, P. *Chem. Phys.* **2006**, *322*, 193.
(22) Welack, S.; Schreiber, M.; Kleinekathöfer, U. *J. Chem. Phys.* **2006**, *124*, 044712.
(23) Fainberg, B. D.; Jouravlev, M.; Nitzan, A. *Phys. Rev. B* **2007**, *76*, 245329.
(24) Bergman, D. J. *Phys. Rev. B* **1979**, *19*, 2359.
(25) Nordlander, P.; Oubre, C.; Prodan, E.; Li, K.; Stockman, M. I. *Nano Lett.* **2004**, *4*, 899.
(26) Fainberg, B. D.; Sukharev, M.; Park, T.-H.; Galperin, M. *Phys. Rev. B* **2011**, *83*, 205425.
(27) Shishodia, M. S.; Fainberg, B. D.; Nitzan, A. In Plasmonics: Metallic Nanostructures and Their Optical Properties IX. *Proceedings of SPIE*, Stockman, M. I., Ed.; SPIE: Bellingham, WA, 2011; vol. *8096*, p 8096 1G.
(28) http://www.lumerical.com/; Lumerical Solutions, Inc.: Vancouver, B.C., Canada.